Intraseasonal variability of the ocean – atmosphere coupling in the Gulf of Guinea during boreal spring and summer

Gaëlle de Coëtlogon (1), Serge Janicot (2) and Alban Lazar (2)

December 19, 2008

Submitted to Quarterly Journal of Royal Meteorological Society

Corresponding author address:

(1) CETP/IPSL, UPMC 10 – 12 avenue de l'Europe 78140 Vélizy – Villacoublay (email: gdc@cetp.ipsl.fr).

(2) LOCEAN/IPSL, IRD, UPMC, Paris.

Abstract

Statistical analyses of the satellite TMI Sea Surface Temperature (SST) and QuikSCAT surface winds in boreal spring and summer are performed to investigate the intraseasonal variability of air-sea interactions in the Gulf of Guinea. EOF decompositions show the existence of peaks around 15 days in their variance spectrum, and their lagged cross-correlation shows the signature of a negative feedback. Lagged linear regressions are performed onto an SST index of the equatorial cold tongue. A cold SST anomaly is forced after about one week by stronger-than-usual southeasterlies linked to the Santa Helena anticyclone, suggesting that the bi-weekly variability is connected to large-scale fluctuations in the South Atlantic. Between about 5°S – 5°N, the SST feedback mechanism described by Wallace, Mitchell and Deser (1989) in the eastern Pacific appears to strongly dominate near-surface atmosphere conditions. When the wind leads the SST, this mechanism explains the stronger monsoonal winds north of 2°N, which bring more humidity and rainfall toward the continent. When the SST leads the wind, it explains the reversal of anomalous winds within about one week and a large part of the bi-weekly variability. Importantly, there is no evidence of the SST influence on local winds through horizontal pressure gradient, as in Lindzen and Nigam (1987). At last, further investigations with an ocean model emphasize the role of horizontal advection in shaping the intraseasonal SST signals. Hence the time-evolution of the wind intraseasonal response to the SST is strongly tight to horizontal ocean dynamics.

1 – Introduction

Li and Philander (1997) suggested that in the Gulf of Guinea, the sea surface temperature (SST) is a passive response of the ocean to seasonal winds, the latter being themselves a passive response to seasonal temperature changes in the West African continent. In contrast, it is commonly thought that the interannual variability of the Atlantic equatorial upwelling, or "cold tongue", and the associated meridional SST gradient over the Gulf of Guinea, play a role in the northward shift of the African Monsoon and the intensity of the related rainfall (Lamb 1978a,b, Opoku-Ankomah and Cordery 1994, Kouadio et al. 2002, Sultan and Janicot 2003, Gu and Adler 2004) through ocean-atmosphere interactions. This concept is generally associated with the seasonal setting of the cold tongue: the strengthening of easterlies lowers the SST and intensifies the SST gradients, increasing in turn the equatorial easterly winds. Through which feedbacks (thermodynamic or dynamic, local or remote) and with which timescales the equatorial SST field influences the equatorial winds in the Atlantic is a much debated and still unsolved question. Contradictory results, past and recent, appear far away from converging. Most of the air-sea interactions studies, based on models or observations, focused on the importance of heat flux feedbacks, but provided incompatible estimates ranging from strongly or weakly negative in observations, reanalyses and some models (Frankignoul et al. 2004) to positive in other models (Chang et al. 1997, Huang and Shukla 2005).

Less is certain regarding the more complex dynamic feedbacks involving ocean dynamics, especially in the equatorial Atlantic. In this basin, Keenlyside and Latif (2007) recently diagnosed in observations and reanalyses the viability of the Bjerknes feedback, but found no evidence of SST effects on the winds, which is a major part of the retroaction loop. Another loop, involving in particular upwelling and sea level pressure (SLP) coupling, is suggested by conceptual models and atmospheric general circulation models (AGCM) as an explanation for the spring westward co-propagation of SST and zonal winds (Mitchell and Wallace 1992, Xie 1994, Nigam and Chao 1996, Okomura and Xie 2004). Its existence and importance in the real climate system remains to be verified.

These feedbacks are thought to happen at short timescales of less than one month or two, due to the fast dynamical response of equatorial atmosphere and ocean. However, whereas studies of air-sea interactions in the Tropical Atlantic are numerous for seasonal and longer timescales, the corresponding intraseasonal variability is still poorly documented. For the atmosphere, Foltz and McPhaden (2004) underlined that Trade winds in the tropical Atlantic vary considerably on timescales of one to two months, with oscillations south of 10°S associated with coherent surface wind and pressure patterns spanning the entire South Atlantic, and along the equatorial band with the Madden - Julian Oscillation. With satellite observations and modelling, Han et al. (2008) and

Polo et al. (2008, 2009) evidenced that intraseasonal variability in the tropical Atlantic Ocean is dominated by the local wind forcing over the central Equator, and by equatorial and coastal waves in the eastern basin. Caniaux et al. (2008) recall how the formation of the cold tongue is a response of the oceanic upper layer to southeastern Trade winds associated with the St Helena anticyclone. Marin et al. (2008) noted that the intense cold tongue in 2005 coincides with a steep meridional thermocline, and advocated that the 2005-2006 SST differences in boreal summer was mainly controlled by the local effect of winds and subsurface oceanic conditions. The correlation between the cold tongue development and the thermocline variability hints at the role of near-surface oceanic processes in the eastern tropical Atlantic. For example, Barreiro et al. (2005) suggested that ocean dynamics play a fundamental role for the prediction of sea surface temperature anomalies (SSTA) in the equatorial and southern tropical Atlantic, and of seasonal rainfall anomalies associated with variations in the intertropical convergence zone (ITCZ) during boreal spring. In their model, the subsurface vertical heat flux due to the anomalous Ekman pumping was a dominant factor of the equatorial SST variability. More specifically, in the eastern Equator near 10°W (the region studied in the present paper), the contribution of subsurface vertical processes in the seasonal cycle was confirmed and coherently estimated with heat budget analyses of observations (Foltz et al. 2003) and ocean general circulation models (OGCM) (Zhou and Carton 1998, Peter et al. 2006). At last, many of these works underscore the modulation of the SST variability by horizontal currents and turbulence.

Regarding the influence of equatorial SST on the local atmosphere at short timescales, three main mechanisms have been proposed. A first mechanism is based on the pressure gradient in the near-surface atmosphere induced by the SST gradient: vertical mixing is supposed to be negligible, while SST-induced air temperature variations within the planetary boundary layer are the major cause of surface pressure variations that drive surface flow over cool tropical regions where SST are below the convective thresholds. Linear dynamics of this mechanism have been described in Lindzen and Nigam (1987, hereafter LN87), Mitchell and Wallace (1992) or Young (1987). Its nonlinear dynamics have been discussed in Tomas et al. (1999). A second mechanism relies on elevated latent heating by convection, which is thought to be a major driver of equatorial surface winds (Gill, 1980, hereafter Gill80). One possible trigger of convection is the SST through vertical mixing, as first considered by Philander et al. (1984) and Gill (1985): a warm SSTA favors convection and thus convergence of surface winds. Note that the response of the wind to a SSTA is expected to be qualitatively similar for both mechanisms and thus hardly differentiable. In Chiang et al. (2000), and in spite of the calibration of the model with Pacific ENSO and Atlantic interhemispheric situations, zonal winds are driven mainly by convection, whereas the LN87 mechanism is most effective for the meridional flow over strong meridional SST gradients.

Considering the seasonal-mean wind and SST distributions over the equatorial Atlantic, the LN87 mechanism should consequently mainly dominate in the west (where SST is above the convection threshold and the wind zonally oriented), and the Gill80 mechanism in the east (SST often below the convection level, winds with a strong meridional component). A third mechanism involves the vertical mixing and the vertical wind profile in the atmospheric boundary layer, the latter being unresolved in previous mechanisms. It has been proposed by Wallace, Mitchell and Deser (1989, hereafter WMD89) and Hayes at al. (1989): when air from the Southern Hemisphere crosses the cold tongue and blows over the warmer water to the north of the equator, the boundary layer stability increases and inhibits downward turbulent mixing of northward momentum from aloft. This decoupling of surface winds from the stronger winds at heights of 100m or more decelerates the near-surface wind and results in low surface wind-stress over the cold waters. As surface winds cross the SST front toward warmer water north of the cold tongue, the convection driven by the enhanced surface heat fluxes increases the downward flux of northward momentum from aloft and accelerates surface winds toward the north. The downwind acceleration results in a divergence of the surface wind field over the northern SST front. In the eastern Pacific, with high-resolution satellite data, Chelton et al. (2001) showed the remarkable spatial and temporal coincidence between surface wind-stress perturbations and the SST, which oscillates with tropical instability waves (TIW) at intraseasonal timescales. For the first time in data entirely independent of AGCM outputs, these authors evidenced the dominance of the WMD89 mechanism at intraseasonal timescales. Most of the studies based on vertical soundings of the atmosphere support the validity of this mechanism (WMD89, Bond 1992, Anderson 2001, Hashizume et al. 2002).

The goal of this work is to provide a statistical basis for the analysis of spring and summer air – sea interactions in the Gulf of Guinea at intraseasonal timescales, based on observations with very high temporal and spatial resolution, thanks to the satellite products now available on periods long enough to establish climatologies. It corresponds to the time when the ITCZ migrates from its southernmost (around the Equator) to its northernmost latitude (around 10°N), and when most of the above thermodynamic and dynamic feedback loops are considered active.

2 – Data

2.1 - SST and surface winds

QuikSCAT winds and TMI SST data were retrieved from Remote Sensing Systems website (www.remss.com), sponsored respectively by the NASA Earth Science REASoN DISCOVER Project and Ocean Vector Winds Science Team. Four main datasets covering two different regions with different resolutions were constructed from the original datasets. The first covers the Gulf of

Guinea (18°W-13°E / 10°S – 10°N) on the original ¼° grid. The second covers the South Atlantic (80°W – 20°E / 37°S – 37°N) and is interpolated on a 1° grid. Only data from 2000 to 2007 were extracted, covering a period of 8 years, sufficient for establishing climatologies at intraseasonal variability. Retrieved data were daily, but filtered with a 3-day running mean due to the lack of daily overlapping satellite tracks. Remaining missing points (presence of clouds) were filled using a cubic spatial interpolation and a few missing days were completed with temporal linear interpolation at each grid points. Total Column Water Vapour (thereafter TCWV) was also retrieved from the TMI data and treated similarly.

The surface wind stress was computed from the surface winds direction and velocity, using the bulk aerodynamic formula $\vec{\tau} = \rho \cdot C_d \cdot \vec{v}_{10} \cdot v_{10}$, where ρ is the air density (taken here to be 1.025 kg/m^3) and C_d is the drag coefficient for neutrally stable conditions. The latter was computed using the modified Large and Pond (1981) drag coefficient described in the appendix of Large et al. (1994), which is the formulation most commonly used for scatterometer applications.

2.2 - ECMWF data

SLP, Geopotential Height at different pressure levels, Surface Solar Radiation (SSR), Surface Latent Heat Flux (SLHF) and Total Column Water Vapour (TCWV) with a resolution of 1.125° from the ECMWF ERA40 reanalysis were retrieved thanks to the ClimServ data server (climserv.ipsl.polytechnique.fr), and the 4-daily data were daily averaged. As the ERA40 data are available only until mid-2002, the same fields were retrieved from the ECMWF meteorological products from the operational analysis over global area over the period mid-2002 / 2007. This use of two different kinds of data (reanalysis over 2000 – 2002 and operational analysis over 2002 – 2007) is of course problematic; however, the results were still more interesting than using other reanalysis products which would have been complete over 2000 – 2007 but with a poorer spatial resolution.

2.3 - TRMM rainfall product

Daily mean precipitations in 2000 – 2007 from the TRMM 3B42 product incorporate several satellite measurements including the TMI and TRMM Precipitation Radar to calibrate infrared precipitation estimates from geostationary satellites (Huffman et al. 2001). They were retrieved from their website (trmm.gsfc.nasa.gov).

2.4 - Oceanic data

A MERCATOR simulation on its most recent configuration, Orca025_lim-T09, was chosen because of its high horizontal (0.25°) resolution and its 3-day out frequency. It was forced by the ECMWF surface data (see Garric 2008 for further specifications of the simulation). Temperature

and horizontal currents at all levels were available from 2000 until May 2007. We computed SST and surface currents in March to August (MAMJJA) in averaging the temperature and currents from the surface layers where the temperature varies less than 0.2°C (note that the use of a 0.5°C criterion did not change the results significantly).

3 – Seasonal evolution of the air-sea interface

Figure 1 shows the monthly means of SST, spatially smoothed precipitation and surface wind during March - August for 2000 – 2007. In March - April, the SST displays a broad meridional gradient (from 27 and 31°C) in the Gulf of Guinea. The ITCZ is also quite broad and covers the northern part of the region, with relatively modest precipitations. The latter are maximum around 3°N west of 10°W where southerlies meet northerlies. Precipitations larger than 1 mm/day correspond to - and are likely influenced by - the warm pool. Hence, in partial agreement with the Gill80 solution, the associated wind-stress field appears clearly tight to convection, as the distribution of its magnitude north of the Equator is inversely proportional to precipitations, i.e. to vertical velocities. In addition, the nascent coastal upwelling and easternmost cold-tongue (not yet visible in the mean SST) starts to reduce the wind speed locally through the WMD89 mechanism.

Then, the northward migration of the ITCZ brings stronger winds northward, setting on the equatorial upwelling. From May to June, the SST progressively cools in the whole equatorial and southern part of the area, with a minimum in the latitudinal band between 4°S and 1°N and near the southern coast of Africa. South of the Equator, the atmospheric boundary layer is evidently locally influenced by the colder SST. Indeed, minima in the wind-stress magnitude and the SST clearly coincide, suggesting that the mechanism of WMD89 dominates at seasonal timescale, e.g. that surface winds decelerate (accelerate) over the colder (warmer) SST. Note that this dominance is associated with the absence of any important convection, thus of any wind induced by convective heating as in the Gill80 mechanism. And no signal of the LN87 mechanism is either found in this area.

North of the Equator and over the whole longitude range, still in May – June, the wind first accelerates from the Equator to about 4°N and then decelerates northward, with a notable maximum at about 2°N from 10°W to 0°E. This quasi-zonal feature is similar to the one observed in the eastern Pacific by LN87 and later publications. Note that the presence of the southern West-African coast increases the temperature gradient between the equatorial cold tongue and the highest northern SST and soil temperature, which surely participates in a large-scale increase of the SLP gradient north of the cold tongue and would favor southwesterlies toward the continent. However, it is remarkable that the wind decreases further north, as it does in the Pacific. This questions the

hypothesis that SST alone controls the SLP, and suggests that the intense convection starting around 1°N-2°N is also at stake. Actually, the large meridional-wind acceleration and deceleration are coherent with precipitations following the Gill80 model: the wind accelerates over the equatorial front of precipitations, and decelerates within the region of maximum precipitations in favor of vertical winds. Only the local increase over 6.10^{-2} $N.m^{-2}$ (yellow stripe in Fig. 1, right panel, May-June) is not related to the precipitation distribution and could need the LN87 model for a better understanding. Overall, the May-June situation is very comparable with that in the eastern Pacific as shown most recently by Chelton et al. (2001) with the same wind and SST dataset (their Figure 1). Note that since convection could be favored by the meridional SST front according to Tomas et al. (1999), the question on the role of SST gradients stays wide open.

Finally, the July-August provides an important complementary picture relative to the previous months, when the deep convection and its associated wind-forcing mechanism leave the place. As expected from the previous considerations, the control of the wind is solely made through the WMD89 mechanism: the wind-stress magnitude is extremely well correlated to the SST over most of the domain. Importantly, along the Equator, whereas the meridional SST gradient keeps approximately the same intensity as in May - June, the 6.10^{-2} $N.m^{-2}$ wind-stress maximum splits in two from its May – June position, and is displaced eastward and westward, following the warmest SST and intense precipitations. This lowers the importance granted to the LN87 mechanism for this maximum, since the departure of the deep convection right from the 10°W-0°E area noted above is accompanied by a decrease of the winds there, despite comparable or stronger SST gradients. However, with or without convection, the large zonal band over 5.10^{-2} $N.m^{-2}$ in May-June and July-August (green stripe, Fig. 1, right middle and lower panels) may still be caused by a large-scale increase of the SLP over the cold tongue, or alternatively by the warmer SST favoring vertical mixing of momentum. With the present dataset, it is impossible to decipher between the two possible mechanisms at this very latitude.

4 – Statistics of the air – sea interaction in the Gulf of Guinea

In order to focus on shorter timescales, SST and surface wind-stress data were filtered using a Lanczos high-pass filter with a 90-day cutoff, thereby removing seasonal and longer timescales. Days from 1st of March to 31st of August were then selected (2000 – 2007) and an Empirical Orthogonal Functions (EOF) decomposition performed on both fields. The first modes of variability catch more than 14% of the total SST variance and almost 20% of the total wind stress (Fig. 2), when second modes catch each less than 6% (not shown). This clear separation between first and second modes attests of the good significance of the first modes: the dominant variability of SST in

this region at the intraseasonal timescales is described by the fluctuations of a more or less intense equatorial SSTA, located on the northern front of the mean cold tongue, where the mean SST meridional gradient is maximum (Fig. 2) and hence favorable to large temperature advection anomalies. The leading mode of the wind stress corresponds roughly to fluctuations in the strength of southeasterlies. Note that the direction of the latter (Fig. 2) is very close to the direction of the mean surface wind-stress (Fig. 1) south of the Equator, but orthogonal to the northeastward monsoonal fluxes close to the northern coast of the Gulf of Guinea.

A lagged cross-correlation between the principal components suggests the existence of a very strong link between these two modes (Fig. 3). A high correlation (more than 0.4) is found when the wind stress leads the SST by 5 days, implying that anomalously strong (weak) southeasterlies lead an intensification (relaxation) of the equatorial upwelling by a few days, with a maximum at lag -5. A strong negative correlation is also found around lag 3, meaning that a decreased (increased) equatorial upwelling, thus warmer-than-normal SST conditions in the cold tongue, leads a weakening (strengthening) of the southeasterlies by a few days (minimum at lag 3). This could describe a negative feedback between the leading modes of SST and wind-stress fluctuations at these short timescales: a "wind burst" in the southeasterlies is followed by a cooling of the equatorial SST within a few days, then the colder SST is followed in turn by a strong decrease of the overlying wind stress in about 3 days, likely through the mechanism of WMD89.

However, this statistical relationship between the two fields does not prove that the SST influences the overlying wind stress at this spatial scale. Indeed, a periodicity of about 15 days is clearly visible in this lagged correlation, as the negative correlation is found again around lags -13 and 16 (Fig. 3). This periodicity in the winds of the Gulf of Guinea, found in some studies (Grodsky and Carton 2001, Mounier et al. 2008), could alone explain a large part of the bi-weekly periodicity observed in the wind / SST lagged cross-correlation. A peak in the 11 – 17 day band was indeed found in the power spectrum of the surface wind-stress principal component (Fig. 4, top), with a strong statistical robustness, the latter having been tested against the spectrum of one thousand AR-1 timeseries with the same variance and short persistence (and beforehand similarly filtered with a 3-day running mean and 90-day high-pass filtering). Thus, a strong bi-weekly periodicity is actually present in intraseasonal fluctuations of the surface wind-stress in the Gulf of Guinea, which could explain a large part of the negative correlation found at lag 3 in Fig. 3. A mere passive oceanic response to the bi-weekly wind fluctuations would exhibit a spectrum with a variance peak on similar frequencies. Though, the spectrum of the SST principal component shows an increased variance over a slightly wider spectrum (11 – 24 days) (Fig. 5), suggesting that oceanic processes could play a role in responding to the wind-stress forcing.

Such a bi-weekly variability could derive from a local ocean-atmosphere feedback (appearing to be negative at short timescales) in the Gulf of Guinea, or alternatively from the atmospheric circulation variability on a larger spatial scale, less dependent upon east-equatorial SST. The large scales will be first examined in the next section, and more details presented at the regional scale in the section after.

5 – Atmospheric signal linked to the northeastern equatorial SST

An index of SST intraseasonal oscillations on the northern front of the cold tongue (thereafter CTI, as "cold tongue index") was built by averaging the filtered SST in the 8°W-4°W / 0.5°S – 1°N area (see framed area in Fig. 2). This region was chosen since it corresponds to the maximum of SST variance at the intraseasonal timescales, as seen in the first EOF pattern (Fig. 2) or the root mean square map of intraseasonal MAMJJA SST (not shown). Lagged regressions of different unfiltered fields onto this index provide a useful insight on the linear relationship between intraseasonal oscillations of SST in the northern front of the cold tongue and the atmospheric circulation, since it allows for a preliminary sorting of causes and consequences inside the ocean-atmosphere coupling phenomenon. Note that all lagged regressions in this paper are shown as the patterns linearly associated with a negative anomaly of one standard deviation in the CTI, i.e. to a colder-than-normal northern cold tongue of about 1°C.

Lagged regressions of South Atlantic surface wind-stress onto the CTI are plotted in Fig. 5, as well as ECMWF SLP and SST. Lags -6 to -2 show that stronger-than-normal southeasterlies in the Gulf of Guinea are followed by a decrease of SST in the eastern equatorial Atlantic with a minimum reached after about 6 days, in agreement with the EOF correlations in the previous section. Also clearly visible, the response of the SST in the coastal upwelling region along Angola / Namibia is slightly faster. A remarkable feature is that the stronger-than-normal southeasterlies in the Gulf of Guinea clearly belongs to a wide basin-scale pattern, mainly an anomalously strong anticyclonic circulation over the south-Atlantic basin. This surface wind-stress anomaly is in very good agreement with the SLP anomaly, which also shows a statistically significant stronger-than-normal St Helena anticyclone centered around 10°W / 30°S at lag -4. A slight eastward displacement of the anticyclonic cell from lags -6 to -2 can be observed. This pattern is clearly barotropic since it can be found in the geopotential height anomaly as high as 100 hPa, albeit with a westward shift of about 10° of the anomalous anticyclonic circulation centre in the upper atmosphere compared to the surface (not shown). Thus, the anomalous southeasterlies which lead the CTI by a few days are clearly connected to the large-scale fluctuations in the South Atlantic atmospheric circulation.

From lag -1 to 1, the large-scale anticyclone vanishes and a divergent wind-stress pattern appears above the cold SSTA, together with a positive SLP local anomaly, strongly resembling a response to the cold tongue development through the LN87 mechanism, or a Gill80 type response in spring when equatorial SST is still favourable to deep convection. However, a closer look reveals that the largest northward wind-stress anomalies are not actually superimposed to the strongest anomalous SST gradient (see section 6). Furthermore, they seem to decay from lag –1 to 0 whereas the SSTA still grows. Hence, the apparent divergence could be alternatively or partly due to a modulation of the wind forcing pattern by the WMD89 mechanism: right at the Equator, the cold SSTA reduces and reverses progressively the initial wind-stress anomaly, but leaves the atmospheric boundary layer almost free to decay at its own pace on both sides of the cold SSTA. This time evolution will be studied in more detail in the next section.

This progressive reversal in the pattern of the wind-stress anomaly takes place over most of the Gulf of Guinea. Since it occurs about one week after the southeasterlies maximum, it fits with the bi-weekly spectral peak in the wind-stress fluctuations discussed in the previous section. The reversed wind anomalies may also be linked with a large-scale atmospheric circulation, since the wind anomaly in the Gulf of Guinea at lag 4 turns around a cyclonic cell centred around 5°W – 25°S in the eastern half of South Atlantic. A concomitant cyclonic circulation can also be observed in the western half of the basin. Both cells are visible in the regression of surface winds as well as in the SLP anomaly. This suggests that the bi-weekly variability partly comes from the large-scale circulation pattern in the whole South Atlantic, with a stronger-than-normal St Helena's anticyclone giving way to a cyclonic cell after about one week. However, several features contradict this hypothesis. Both surface wind patterns are not exactly linearly opposite, since the cyclonic anomaly at lag 3 is shifted 5° north-eastward with regard to the anticyclone at lag -4. In addition, the east-equatorial signal seems to be dissociated from the anticyclone at lags 0 and 1, before reconnecting to it from lag 2 onwards. Moreover, while the first EOF of surface winds on the whole South Atlantic basin corresponds well to a more or less intense St Helena's anticyclone, it does not exhibit a significant bi-weekly variability (not shown). Thus, the reversal of the surface wind anomaly in the southern hemisphere could rather be in part a response of the whole Hadley cell to the cold SSTA in the eastern equatorial Atlantic, since the positive SLP anomaly over the cold tongue develops slightly in advance of the negative SLP anomaly around 0°-10° E / 20° - 30°S. This is obviously an interesting hypothesis, which will need further investigations when the new ECMWF reanalyses are completed over 2000 – 2007.

In parallel, over the Angola-Benguela upwelling front area (near 10°S-20°S), a much smaller (but significant) positive SLP anomaly also takes place, after a weaker (but significant) cold SSTA

was forced by the wind anomaly which favours upwelling (northward and parallel to the coast) at negative lags. It could be an atmospheric response to the cold SSTA, with an apparent delay of a few days between the SSTA minimum and the SLP significant signal. Although the clear response of the ECMWF model-derived SLP, satellite winds do not show any local reinforcement near the corresponding isobars, as could be expected. This suggests that the reanalysis pressure field is not in very good agreement with the satellite estimates, and that the upwelling intraseasonal SSTA is not strong enough to have a measurable impact on the winds, which obviously needs also further investigations with more appropriate data.

Eventually, the present dataset makes possible to search for elements evidencing or undermining the less obvious constituent of the Bjerknes feedback, e.g. the occurrence of wind bursts in response to equatorial SSTA. These wind anomalies are thought to result from the LN87 or the Gill80 mechanism, and are supposed to be particularly active during the equatorial mode events, in boreal summer or winter (Okumura and Xie, 2006): positive (negative) zonal-wind anomalies in the west of the cold tongue trigger upwelling (downwelling) Kelvin waves that could reinforce the initial SSTA, thus feeding a positive feedback loop. Using monthly mean data, Keenlyside and Latif (2007) show a positive correlation maximum at lag 0 between western-equatorial zonal winds and the ATL3 (20°W-0°) SSTA, located slightly west of the CTI area. In Fig. 5, anomalies of equatorial easterly-wind are indeed found, but only before say lag -2 day, and obviously associated to the hemisphere-scale initial forcing. No signal can be seen when the SSTA peaks (lag 0) and later on (the same is true from lag 6 onwards, not shown). This result indicates that the Bjerknes feedback does not hold for SSTA east of about 10°W at intraseasonal timescales. Moreover, a one-month average of the wind field centred on lag 0 would obviously be dominated over the western Equator by the large signal at negative lags, misleading to the suggestion that the eastern equatorial SSTA triggers western zonal wind bursts: the use of monthly mean data to analyse intraseasonal feedbacks may lead to a wrong interpretation of the air-sea interaction. However, the CTI is only relevant for investigating whether this retroaction takes place or not when the eastern equatorial SSTA develops. An additional analysis focused on the western equatorial SSTA would help to complete the picture.

6 – Regional air-sea feedbacks

The detailed time-dependent patterns of SST and winds are now examined specifically in the vicinity of the maximum SSTA, in the Gulf of Guinea. Fig. 5 exhibits a divergence of the surface wind-stress south of the northern coast from lag -1 onwards, just above the coldest equatorial SSTA. In order to identify the mechanism by which the SSTA influences the near-surface

atmospheric circulation, a zoom of this regression is made between 4°S and 5°N from lag -6 to 9 (Fig. 6).

The temperature in the index area is minimal 5 or 6 days after the maximum anomalous wind forcing (occurring around lag -6 or -5): its persistence is thus around one week. Meanwhile, a small deceleration of the surface winds when passing over the growing cold SSTA can be observed as soon as lag -5, as well as a slight westward deviation of their direction. At lags -4 and -3, these deceleration and westward deviation increase concomitantly with the cold SSTA, whereas the strong winds north of the SSTA start to decay, likely by their own persistence as suggested before. Then, the clear divergence of the surface winds settles at lag -1 on the northern front of the cold SSTA. It clearly results, on one hand, from the inversion of the wind direction over the cold SSTA through the WMD89 mechanism, and on the other hand from the remaining initial wind burst north of 2°N. It is in parallel possible that the cold SSTA increases the mean Equator-to-coast meridional gradient of surface temperature, enhancing the initial northern wind burst through the LN87 mechanism.

South of 2°N, the pattern of the wind-stress anomaly coincides spatially very well with the SSTA, with a small lag of a few days. Indeed, the SSTA maximum (of about $1°C$ at lag 0) is located exactly at the same place than the maximum of the southeastward wind-stress anomaly, which amounts to $0.8 - 0.9 \times 10^{-2} N.m^{-2}$ at lags 1 or 2 and decreases progressively afterwards. From lag 3 onwards, this equatorial cold SSTA splits in two lobe-shaped anomalies on both sides of the Equator, and a southeastward wind-stress anomaly persists over the southern lobe of this SST pattern with a good agreement in locations of maximum. Meanwhile, a warm SSTA settles between 3°W and 0° at lag 6 and increases until lag 9, coming with a northward anomaly of surface wind-stress perfectly matching the SST pattern. This striking similarity between anomalous SST and wind-stress magnitude strongly suggests that the mechanism described by WMD89 contributes to the wind anomalies in the first place. Indeed, the mean surface wind-stress is mainly northwestward in this region (Fig. 1): a cold SSTA decelerating the wind would create a southeastward wind anomaly, while a warm SSTA would create a northwestward anomaly, exactly as shown in Fig. 6 and described previously. This emphasizes the importance of the WMD89's mechanism at intraseasonal timescales during boreal spring and summer in the eastern equatorial Atlantic, since it may lead to the local negative feedback observed between the SST and surface winds, and to the bi-weekly variability of the wind strength in this region.

North of about 2°N, anomalous strong southerlies dominate. They belong to the large-scale pattern of wind at first (Fig. 5), and persist from lag -4 until lag 3 or 4 with a 90° clockwise rotation: starting northwestward, they turn mostly northward around lag 0, and then northeastward. Because

of this orthogonal rotation, these anomalous winds toward the continent cannot be a statistical artifact coming from the bi-weekly variability of the wind-stress observed in the Gulf of Guinea and could be partly forced by the underlying SSTA. While the mechanism of WMD89 is also probably at work there, with the northern front of the cold SSTA accelerating the surface wind with a lag of a few days, it cannot simply explain the change in the direction of the winds. The latter could be rather due to the SLP gradient between the cold tongue and the continent generated by the SSTA, following the mechanism described in LN87. This is supported by the significant anomalous high SLP observed above the cold anomaly from lags 1 to 5 (Fig. 5), and the fact that this anomaly is visible in the geopotentiel height anomaly up to 700 hPa, albeit hardly significant (not shown). Northward at first, when the SLP gradient between the ocean and the continent is still weak, the winds turn progressively eastward, strained by the Coriolis deviation around the increasing SLP anomaly.

Thus, on the northern front of the SST gradient, increased monsoonal fluxes are directed toward the continent from lags -5 to 4. As can be easily foreseen, these winds increase the transport of humidity, i.e. precipitable water, over the West African continent. Fig. 7 (colours) shows the regression of the TRMM precipitation onto the CTI, exhibiting increased rainfall widely spread along the West African coast from lags -5 to 1, when the northward monsoonal winds are the strongest. TCWV is also projected on the CTI (Fig. 7, black contours) and fits very well with the precipitation anomalies: increase in the latter comes naturally with an increase of the TCWV, mostly contained in the atmospheric boundary layer. Thus, an anomalous high TCWV is centred on the southern coast of West Africa, reaches its maximum northward extension (8°N) in the 5°W - 5°E longitudinal band around lag -2, and persists until lags 3 or 4.

No significant correlation of the rainfall with the CTI are found north of 8°N, as could have been expected from previous studies, such as Okomura and Xie (2004)'s: as the precipitation comes only in late summer so far north, it cannot be detected by our analysis covering the March – August period. A deficit of rainfall is also observed between 5°W – 10°W along the Equator from lags 1 to 3 and could be due to the ITCZ pushed northward by anomalous southerlies.

A westward displacement of the large positive rainfall and TCWV anomaly is observed in the 5°N – 10°N band from lags -3 to 5 and develops surprisingly while the anomalous monsoonal fluxes turn eastward, which eliminates any local explanation. It could rather be linked to the warm SST anomaly observed in Fig. 5 in the same zonal band. But as the latter does not exhibit the same westward propagation, it is more probably forced by fluctuations of the large-scale atmospheric circulation, as would be the anomalous strong rainfall pattern coming with an anomalous high TCWV off the northeast of Brazil from lag 3 onwards. The coastal rainfall seems to peak (at lags –4

and –3) and decrease in phase with the northern wind anomaly, but the latter decays without moving westward, which rather excludes any link between the two fields. Further investigations are needed about these important issues and would be possible with a complete reanalysis of atmospheric data.

7 – Origin of SST anomalies

The SSTA is created through thermodynamical air-sea exchanges at the sea surface, horizontal oceanic advection, and vertical processes of heat exchange at the base of the oceanic mixed-layer. In our case, and keeping only significant terms, the SSTA equation can thus comes down to: $\frac{\partial T'}{\partial t} = -\overline{U}.\Delta T' - U'.\Delta \overline{T} + Q' + We' + Kv'$, where T' is the SSTA, $\overline{T}$ the mean SST in MAMJJA, U' the current anomaly with zonal (*u'*) and meridional (*v'*) components, $\overline{U}$ $(\overline{u}, \overline{v})$ the mean current in MAMJJA, *Q'* the term of anomalous net surface heat flux, *We'* the term of anomalous Ekman pumping and *Kv'* the term of anomalous vertical diffusion. We discuss here which of these processes may be the most important in forcing the cold northern equatorial SSTA (i.e. the CTI used in this study) at intraseasonal timescales, and which ones may lead to the characteristic pattern observed in Fig. 6 after lag 3 or 4.

7.1 – Surface heat fluxes

The influence of the sensible heat flux on the SST is generally very small in the Tropics, as well as the long wave radiation. But the latent heat flux could play an important role, in particular through the cooling effect of stronger-than-normal winds, as well as the very intense solar radiation at these low latitudes (Foltz et al. 2003, Peter et al. 2006). In order to estimate the respective parts of latent heat flux and solar radiation in the intraseasonal forcing of the northern cold tongue variability, the corresponding ECMWF data were averaged over the same area as the CTI (8°W – 4°W / 0.5°S – 1°N). No significant correlation was found in the lagged cross-correlation of the solar radiation with the CTI (Fig. 8). Regression maps of the solar radiation onto the CTI show significant correlations along the northern coast of the Gulf of Guinea from lags -5 to 0 (not shown), explained by a more intense atmospheric convection in the ITCZ linked to stronger-than-normal southeasterlies, but far from the strongest SSTA in the northern cold tongue. Thus, the solar radiation does not seem to influence significantly the CTI. Significant correlations between the surface latent heat flux and the CTI were found when the latter leads the flux by a few days, with a maximum at lag 3 (Fig. 8), but not when the flux leads: thus, the surface latent heat flux significantly cools the atmosphere once the cold SSTA is settled but does not seem to contribute significantly to the formation of the SSTA.

7.2 – Ocean dynamics

As no significant influence of the air-sea fluxes have been detected in the formation of the cold SSTA, oceanic processes must play the leading part. Further insights in the ocean dynamics have been made with the forced MERCATOR simulation, in which the mean MAMJJA SST is very close to the observations plotted in Fig. 2. An index similar to the CTI was computed in MERCATOR with the SST data averaged over the same area (8°W – 4°W / 0.5°S – 1°N). The linear regression of the SST to this index is plotted in Fig. 9 (first column). The amplitude of SSTA is slightly smaller than in observations (Fig. 6), probably due to the fact that the area of average for the CTI does not correspond exactly to the maximum variance of SST in MERCATOR as it is the case in the observations. Besides that, a striking similarity is observed between the two SST regressions: the large equatorial SST cold anomaly, maximum at lag 0, has a kind of westward propagation from lags -6 to 15. Meanwhile, it splits in two lobe anomalies on both sides of the Equator after lag 3. A warm anomaly, which seems to follow the cold anomaly, appear between 3°W and 0° at lag 6 with the same apparent westward propagation. This good agreement between observations and simulation suggests that the model reproduces well the ocean dynamics behind SST fluctuations. The model is forced by ECMWF surface fields, and the surface wind-stress linked to the CTI in MERCATOR is quite close to the high-resolution satellite wind forcing, with a reversal of the winds in the southern half of the domain after about one week (Fig. 9, right column).

Both propagation velocity and pattern of SST remind of a slow westward-propagating Rossby wave. But this characteristic pattern seems to have a cycle of about 20 day length, since the coldest SSTA at lag 0 is replaced by a warm SSTA at lags 9 – 12, and no corresponding long Rossby wave mode can be found in this region between roughly 10 and 35 days of periodicity (Athié et al., 2008). A mixed Rossby-gravity wave, or Yanaï wave, may possibly takes place here, but the examination of the Topex / Poséïdon sea surface height anomalies (not shown) undermines clearly this hypothesis since no propagating pattern having an equatorial wave distribution was found. We therefore now study the vertical and horizontal advection terms.

The first term that comes naturally to mind when searching for the cause of a SSTA within the equatorial upwelling is the vertical advection by the Ekman pumping. Here, in addition of using a theoretical estimate based on the wind anomaly, the divergence of anomalous horizontal surface currents ($\frac{\Delta u'}{\Delta x} + \frac{\Delta v'}{\Delta y}$, thereafter HDIV) was computed, and linearly regressed to the MERCATOR CTI (Fig. 9, third column). The HDIV pattern is in good agreement with the regression of the theoretical Ekman pumping (not shown): stronger-than-normal southeasterlies create the divergence of surface oceanic currents between roughly 4°S and the Equator at lags -6 and -3, and piles up the

surface waters against the northern coast of the Gulf of Guinea, thereby creating a convergence north of around 1°N. Then, this pattern reverses between lag 0 and 3. Although the HDIV pattern is compatible with the cooling of SST between the Equator and 4°S at lags -6 and -3, the convergence of surface currents, observed to be maximal north of about 1°N at lag -3, cannot explain the very strong equatorial cooling of SST at lags -3 and 0 between 1°N and 3°N. Moreover, in the same area, the HDIV is divergent at lag 6 and 9, thus would rather tend to damp the warm SST anomaly, while the latter increases. Thus, other oceanic processes must control the signal.

Horizontal advection of the mean SST by anomalous currents was then computed, using the simple scheme: $u'\frac{\Delta\overline{T}}{\Delta x}+v'\frac{\Delta\overline{T}}{\Delta y}$, *u'* and *v'* being the surface current anomaly and $\overline{T}$ the mean SST in MAMJJA. The regression of this field ($-U'.\nabla\overline{T}$, Fig. 9, second column) to the CTI is in a much better agreement than HDIV with the temporal evolution of the SST. From lag -6 to 0, anomalous surface currents (Fig. 9, second column) result from a mainly meridional wind-stress anomaly in the presence of no or little Coriolis effect. Fastest currents are comprised in the equatorial region between 1°S and 2°N, probably because the mixed-layer is shallower there. They transport northward colder water from the seasonal-mean cold tongue spanning south of the Equator (see Fig. 2) and cool the equatorial SST between 0 and 2°N. The cold SSTA grows up to 0.5°C in about 6 days, while the order of magnitude of $-U'.\nabla\overline{T}$ is around $8.10^{-7}°C.s^{-1}$ at lag -3, corresponding to $0.4°C$ for six days: it forms obviously the essential part of the initial SSTA, in particular to the expense of the vertical turbulence.

At lags 3 and 6, southward anomalous currents take place along the northern side of the Equator. The link between these currents and the wind-stress anomaly is less clear than in the case of the northward currents at lags -6 and -3, but taking into account the delay of the oceanic response, the reversal of the wind anomalies coincides well with the reversal of the currents. They bring back warmer water, thereby increasing the temperature and leading to the warm SSTA in the 5°W – 5°E northern-equatorial band. The narrowness of the most intense warming effect of horizontal advection, obviously maximum between the Equator and 2°N (where the mean SST gradient is maximum), explains the splitting of the wide SSTA in two lobes on both sides of the Equator. Eventually, in the northern lobe, both HDIV and divergence would combine to increase the cold SSTA, which is maximal at lag 12.

The horizontal advection of anomalous SST by the mean current was finally estimated by computing $\overline{u}\frac{\Delta T'}{\Delta x}+\overline{v}\frac{\Delta T'}{\Delta y}$, $\overline{u}$ and $\overline{v}$ being the mean surface current in MAMJJA and T' the SSTA. The linear regression of this field ($-\overline{U}.\nabla T'$) to the CTI was plotted in Fig. 9 (fourth column). It is

generally less important in magnitude than the regression of $-U'.\nabla\overline{T}$. However, the westward displacement of the SST pattern observed in Fig. 9 (left) fits well with this regression. SSTA just north of the Equator move by about 7° westward from lags -6 to 15, i.e. with a velocity of 40 – 50 $cm.s^{-1}$ which is typical of the southern-equatorial current between the Equator and 2°N (Fig. 10). The westward propagation of SSTA is thus compatible with the advection by the mean currents. The shift of the southern cold lobe at lags 9 and 12 compared to the northern one would thus be due to the weaker westward mean surface currents around 2°S.

We did not evaluate the contribution of the small grid-scale parameterization of the turbulence, in particular the lateral processes, and hence our budget is not close. Nevertheless, this budget is likely dominated by large-scale processes on the horizontal plane. Therefore, we conclude that the intraseasonal cold and then warm SSTA studied in the present paper are mainly the result of an advective modulation of the mean equatorial cold tongue, which is not surprising since the reference area for the highest intraseasonal variance is in the northern front of the cold tongue, where the meridional SST gradient is maximum.

8 – Summary and discussion

Air-sea interactions occurring within the Gulf of Guinea during boreal spring and summer are analyzed with high-quality satellite estimates of SST, surface wind-stress and precipitations. The results provide model-independent evidences of air-sea interactions and couplings, and an accurate OGCM simulation helps to understand the time evolution of the SST field.

During boreal spring and summer in the eastern-equatorial Atlantic, seasonal means provide enlightenments for the three main mechanisms of the SST influence on surface winds: the SST affects the convection that generates surface winds (Gill 1980, Philander 1984, Gill 1985), SST gradients control the SLP and hence the winds (Lindzen and Nigam, 1987), and the SST conditions the boundary-layer vertical mixing that modulates surface winds (Wallace, Mitchell and Deser, 1989). However, the latter mechanism largely dominates in the Gulf of Guinea, particularly in dry conditions (say when precipitations do not exceed 1 mm/day) and between 5°S and 5°N, when the agreement between SST and wind distributions is very high. This study of the SST and surface-wind interaction away from intense rain is similar to the Chelton et al. (2001)'s analysis in the eastern-equatorial Pacific. From March to June, when the ITCZ lies down the Equator and then the northern Gulf of Guinea, there are robust evidences for a modulation of the surface wind distribution by deep convection following the Gill80 model. The convection itself is well correlated with the SST, which is believed to influence it, and hence indirectly the winds.

At intraseasonal timescales, the highest EOF mode of SST variability during the March-August period in the Gulf of Guinea is dominated by a strong zonal anomaly straddling the Equator on the northern front of the cold tongue, where the mean SST gradient is the largest. The highest mode of the surface wind-stress variability corresponds to stronger or weaker southeasterlies. Both modes are highly correlated at a few days lag, exhibiting a negative feedback and a strong periodicity of about two weeks. Note that the two dominant coupled modes of variability in spring and summer are the interhemispheric mode and the equatorial one, but the SST EOF pattern which frames our study resembles more the second mode. It is due to the highest amplitude, in the eastern Atlantic, of the equatorial mode relative to the interhemispheric mode. Hence, the region and the period chosen in the present study provide new informations about the high-frequency time evolution of equatorial and southern Atlantic air-sea interactions, which likely rather pertain to the category of equatorial-mode variability. This point is supported by the patterns of the basin-scale regressed SSTA. A more seasonalized analysis could better separate processes in terms of these modes.

The reference SST index corresponds to the highest intraseasonal SST variability within the Gulf of Guinea for the spring and summer period. Lagged linear regressions were performed onto this index. The stronger southeasterlies leading to a colder-than-normal northern equatorial SST belong to a wide anticyclonic cell over the South Atlantic basin. This is consistent with the observations of Caniaux et al. (2008) or Marin et al. (2008) who suggest that the "wind bursts" leading to the cold equatorial SST in 2005 result from the variability of the St Helena anticyclone. Then, the reversal of anomalous winds in the Eastern Tropical Atlantic after about one week could be linked to the synoptic fluctuations of the large-scale atmospheric circulation in the South Atlantic, following a non-linear cycle. Another possibility is that this reversal would come from a large-scale atmospheric response (Hadley cell) to the SST equatorial anomaly. While these propositions need to be further investigated with more appropriate data, we suggest that the cold SSTA in the eastern Tropical Atlantic reverses in the first place the equatorial pattern of anomalous southeasterlies after about one week, through the mechanism of WMD89, thereby creating a bi-weekly variability.

This suggestion is supported by a closer view of the surface wind-stress and SST regression in the Gulf of Guinea. Indeed, the latter shows a remarkable agreement between the patterns of anomalous SST and wind-stress magnitude, with a cold (resp. warm) anomaly decelerating (accelerating) the surface winds, according to the mechanism of WMD89. North of 2°N, the cold SSTA also probably leads to a stronger meridional SLP gradient, following the mechanism of LN87, which would increase the southerlies toward the continent and rainfall along the southern coastal regions in West Africa. Further investigations are obviously needed to explore the dynamics

of this atmospheric response to SSTA near the southern coast of West Africa. In particular, the importance of the vertical mixing processes in the atmospheric boundary layer should be investigated as Hashuzime et al. (2002) did in the eastern Pacific for TIW-induced perturbations of the surface wind. New data, such as vertical soundings from the EGEE cruises in 2005 and 2006, or numerical ECMWF reanalysis (ERA interim), would make this study possible.

Thus, around the Equator, stronger southeasterlies force the cooling of the ocean surface and the cooler SST in turn slows down southeasterlies with a lag of about one week. This reversal of the wind strength influences again the ocean surface, as been shown by the linear regressions performed with the outputs of an OGCM forced by ECMWF surface fields. The mechanisms involved in the generation of the SSTA were investigated. Surface heat fluxes (latent and solar radiation) do not seem to have a significant impact, even if a cold SSTA cools the near atmosphere a few days after its generation. The expected importance of the Ekman pumping on the SST evolution was tentatively estimated with the horizontal divergence HDIV field alone, although it is highly questionable since the vertical heat exchange through Ekman pumping depends on the thermocline depth: if the latter is close to the surface, HDIV will have a larger impact on SST evolution than if the thermocline is deeper. However, HDIV anomaly was found here to be generally opposed to the evolution of intraseasonal northern-equatorial SST.

We show that it is in fact essentially the modulation of the cold tongue front by anomalous cross equatorial currents, forced by the anomalous meridional winds, that creates the strongest intraseasaonal variability in the cold tongue. As soon as the anomalous wind reverses, first due to the local retroaction of the SST anomaly and later on to the basin-scale SLP anomaly, the meridional advection of the mean SST by the anomalous currents damps partly the SSTA. It also generates smaller SSTA of opposite signs. The remaining anomalies are then advected westard by the mean current and dissipate.

Note that we do not overlook the importance of vertical advective and turbulent processes, which play a major role in the settlement of the seasonal cold tongue and intraseasonal SST fluctuations in this area (Anne-Charlotte Peter, personal communication). The choice for the location of the CTI, made with objective criteria (largest variance and EOF decomposition), is of course determinant here. The northern front of the cold tongue, as a meridional gradient, produces naturally the highest variance within the whole Gulf, forced by meridional winds and deriving currents. Also, we have qualitatively deduced from the orientation of the anomalous wind and currents that v' was dominated by the Ekman component of the surface current. The geostrophic component could also be non negligible, albeit likely weak in anomaly at such temporal scales. Eventually, a possible mixed gravity – Rossby wave could partly control v': east of 10°W, Han et

al. (2008) show that the sea surface height anomaly and thermocline variations at 10 – 40-day periods result almost entirely from Yanai waves excited mainly by the quasi-biweekly meridional winds, as also suggested in Athié et al. (2008). But our results show that horizontal advection alone can explain at first order the largest intraseasonal fluctuations of the eastern-equatorial SST. They are forced by intraseasonal fluctuations of the winds, a major result of this study being that these fluctuations are largely determined by the WMD89 SST feedback.

Acknowledgments

We are thankful to Jean-Eudes Lombard and Gilles Garric for providing the MERCATOR simulation data, and to Harold F. Pierce for his help to retrieve the TRMM B42 rainfall data. This study was also supported by the AMMA project. Based on French initiative, AMMA was built by an international scientific group and is currently funded by a large number of agencies, especially from France, UK, US and Africa. It has been the beneficiary of a major financial contribution from the European Community's Sixth Framework Research Programme. Detailed information on scientific coordination and funding is available on the AMMA International website http://www.amma-international.org.

The authors would like to thank Jerôme Sirven, Anne-Charlotte Peter and particularly Frédéric Marin for many helpful discussions.

References

Athié, G., and F. Marin, 2008a: Cross-equatorial structure and temporal modulation of intraseasonal variabaility at the surface of the Tropical Atlantic Ocean. *J. Geophys. Res.*, 113, doi:10.1029/2007JC004332.

Barreiro, M., P. Chang, L. Ji, R. Saravanan and A. Giannini, 2005: Dynamical Elements of Predicting Boreal Spring Tropical Atlantic Sea-Surface Temperatures. *Dynamics of Atmospheres and Oceans*, 31, 61-85.

Caniaux, G., H. Giordani, M. Wade, F. Guichard and J. L. Redelsperger, 2008: The St. Helena Anticyclone, the Atlantic Cold Tongue and the African Monsoon. *In prep.*

Chang, P., L. Ji, and H. Li, 1997: A decadal climate variation in the tropical Atlantic Ocean from thermodynamic air-sea interactions. *Nature*, 385, 516–518.

Chelton, D. B., S. K. Esbensen, M. G. Schlax, N. Thum and M. H. Freilich, 2001: Observations of Coupling between Surface Wind Stress and Seas Surface Temperature in the Eastern Tropical Pacific. *J. of Climate*, vol. 14, pp. 1479 – 1498.

Chiang, J. C. H., S. E. Zebiak and M. A. Cane, 2001: On the relative roles of elevated heating and sea surface temperature gradients in driving surface winds over tropical oceans. *J. Atmos. Sci.*, 58, 1371-1394.

Foltz, G. R, S. A. Grodsky, J. A. Carton, M. J. McPhaden, 2003: Seasonal mixed layer heat budget of the Tropical Atlantic Ocean, *J. Geophys. Res.*, 108 (C5), 3146 – 3159.

Foltz, G. R. and M. J. McPhaden, 2004: The 30 – 70 day oscillations in the tropical Atlantic. *Geophys. Res. Lett.*, vol. 31, L15205, doi: 10.1029/2004GL020023.

Frankignoul E. Kestenare, M. Botzet, A. F. Carril, H. Drange, A. Pardaens, L. Terray, and R. Sutton, 2004: An intercomparison between the surface heat flux feedback in five coupled models, COADS and the NCEP reanalysis. *Climate Dyn*., 22, doi:10.1007/s00382-003-0388-3.

Garric, G., R. Bourdalle-Badie, O. Le Galloudec, C. Bricaud, C. Derval, E. Durand and Y. Drillet, 2008: Description of the interannual experiment ORCA025-T09, 1998-2006. *Mercator Ocean Report*, 235, Annexe 2.

Gill, A. E., 1980: Some simple solutions for heat-induced tropical circulation. *Q. J. R. M. S.*, 106, 447-462.

Gill, A. E., 1985: Elements of coupled ocean-atmosphere models for the tropics, Coupled ocean-atmosphere models, edited by J. C. J. Nihoul, *Elsevier Oceanogr.*, Ser., 40, 303-327, Amsterdam 1985.

Grodsky, S.A. and J.A. Carton, 2001: Coupled land/atmosphere interactions in the West African monsoon. *Geophys. Res. Lett.,* 28, 1503-1506.

Gu, G. and R. F. Adler*,* 2004: Seasonal evolution and variability associated with the West African monsoon system. *J. of Climate*, 17, 3364-3377.

Han, W., P. J. Webster, J. L. Lin, W. T. Liu, R. Fu, D. Yuan and A. Hu, 2008: Dynamics of Intraseasonal Sea Level and Thermocline Variability in the Equatorial Atlantic during 2002 – 03. *J. of Phys. Ocean.*, 38, 945—967.

Hashizume, H., S.-P. Xie, M. Fujiwara, M. Shiotani, T. Watanabe, Y. Tanimoto, W. T. Liu and K. Takeuchi, 2002: Direct Observations of Atmospheric Boundary Layer Response to SST Variations Associated with Tropical Instability Waves over the Eastern Equatorial Pacific. *J. of Climate*, 15, 3379 – 3393.

Hayes, S. P., M. J. McPhaden and J. M. Wallace, 1989: The influence of sea surface temperature on surface wind in the eastern equatorial Pacific: weekly to monthly variability. *J. of Climate*, 2, 1500 – 1506.

Huang, B. and J. Shukla, 2005: Ocean-Atmosphere Interactions in the Tropical and Subtropical Atlantic Ocean. *J. of Climate*, 18, 1652-1672.

Huffman, G. J., R. F. Adler, M. M. Morrissey, D. T. Bolvin, S. Curtis, R. Joyce, B. McGavock and J. Susskind, 2001: Global precipitation at one-degree daily resolution from multisatellite observations. *J. Hydrometeor.*, 2, 36-50.

Kouadio, Y., D.A. Ochou, J. Servain, 2002: Atlantic influence on the rainfall variability in West Africa during the years 1950-90. *J. of Climate*, 2, 187-202.

Lamb, P.J., 1978a: Large scale tropical surface circulation patterns associated with Subsaharan weather anomalies. *Tellus*, 30, 240-251.

Lamb, P.J., 1978b. Case studies of tropical Atlantic surface circulation patterns during recent sub-Saharan weather anomalies: 1967 and 1968. *Mon. Wea. Rev*., 106, 482-491.

Large, W. G., J. C. McWilliams and S. C. Doney, 1994: Oceanic vertical mixing: a review and a model with a non local boundary layer parameterization. *Rev. Geophys.*, 32, 363-403.

Large, W.G. and S. Pond, 1981: Open ocean momentum flux measurements in moderate to strong winds. *J. Phys. Oceanogr.*, 11, 324-336.

Li, T. and S. G .H. Philander, 1997: On the seasonal cycle of the equatorial Atlantic Ocean. *J. of Climate*, 10(4), 813-817.

Lindzen, R.S. and S. Nigam, 1987: On the role of sea surface temperature gradients in forcing low level winds and convergence in the tropics. *J. Atmos. Sci.*, 44, 2418-2436.

Marin, F., G. Caniaux, B. Bourlès, H. Giordani, Y. Gouriou and E. Key, 2008: Why were sea surface temperatures so different in the eastern equatorial Atlantic in June 2005 and 2006 ? *Submitted to Q. J. R. M. S.*

Mitchell, T. P. and J. M. Wallace, 1992: The Annual Cycle in Equatorial Convection and Sea Surface Temperature. *J. of Climate*, 5, 1140 – 1156.

Mounier, F., S. Janicot and G. Kiladis, 2008: The West African monsoon dynamics. Part III: The quasi-biweekly zonal dipole. *J. of Climate,* 21, 1911-1928.

Nigam, S. and Y. Chao, 1996: Evolution dynamics of tropical ocean–atmosphere annual cycle variability. *J. of Climate*, 9, 3187–3205.

Okumura, Y. and S.-P. Xie, 2004: Interaction of the Atlantic Equatorial Cold Tongue and the African Monsoon. *J. of Climate*, 17, 3589 – 3602.

Opoku-Ankomah, Y. and Cordery, I., 1994: Atlantic sea surface temperatures and rainfall variability in Ghana. *J. of Climate*, 7,. 551–558.

Peter, A. C., M. Le Hénaff, Y. du Penhoat, C. E. Menkes, F. Marin, J. Vialard, G. Caniaux and A. Lazar, 2006: A model study of the seasonal mixed layer heat budget in the equatorial Atlantic, *J. Geoph. Res.*, 111 (C6), C06014, 10.1029/2005JC003157.

Philander, S. G. H. and R. C. Pacanowski, 1981: Response of Equatorial Oceans to Periodic Forcing. *J. Geophys. Res.*, 86(C3), 1903–1916.

Philander, S. G. H., T. Yamagata and R. C. Pacanowski, 1984: Unstable air-sea interaction in the tropics. *J. Atmos. Sci.* 41, 604-613.

Plaut, G.R. and R. Vautard, 1994: Spells of oscillations and weather regimes in the low-frequency dynamics of the Northern Hemisphere. *J. Atmos. Sci.*, 51, 210-236.

Polo, I., A. Lazar, B. Rodriguez-Fonseca and S. Arnault, 2008: Oceanic Kelvin waves and tropical Atlantic intraseasonal variability: 1. Kelvin wave characterization. *J. Geophys. Res*., 113, C07009, doi:10.1029/2007JC004495.

Polo, I., A. Lazar, B. Rodriguez-Fonseca, 2009: Oceanic Kelvin waves and tropical Atlantic intraseasonal variability: 2. Wave Forcing. *Submitted to J. Geophys. Res.*

Sultan, B. and S. Janicot**,** 2003: The West African monsoon dynamics, Part II : The "pre-onset" and the "onset" of the summer monsoon. *J. of Climate,* 16, 3407-3427.

Tomas, R. A., J. R. Holton and P. J. Webster, 1999: The influence of cross-equatorial pressure gradients on the location of near-equatorial convection. *Quart. J. Roy. Meteor. Soc.*, 125, 1107–1127.

Wallace, J. M., T. P. Mitchell and C. Deser, 1989: The Influence of Sea-Surface Temperature on Surface Wind in the Eastern Equatorial Pacific: Seasonal and Interannual Variability. *J. of Climate*, 2, 1492 – 1499.

Xie, S.-P., 1994: On the genesis of the equatorial annual cycle. *J. of Climate*, 7, 2008-2013.

Young, J. A., 1987: Boundary layer dynamics of tropical and monsoonal flows. *Monsoon meteorology*, Oxford University Press, 461-500.

Zebiak, S. E. and M. A. Cane, 1987: A model El-Niño – Southern Oscillation. *Mon. Wea. Rev.*, 115, 2262 – 2278.

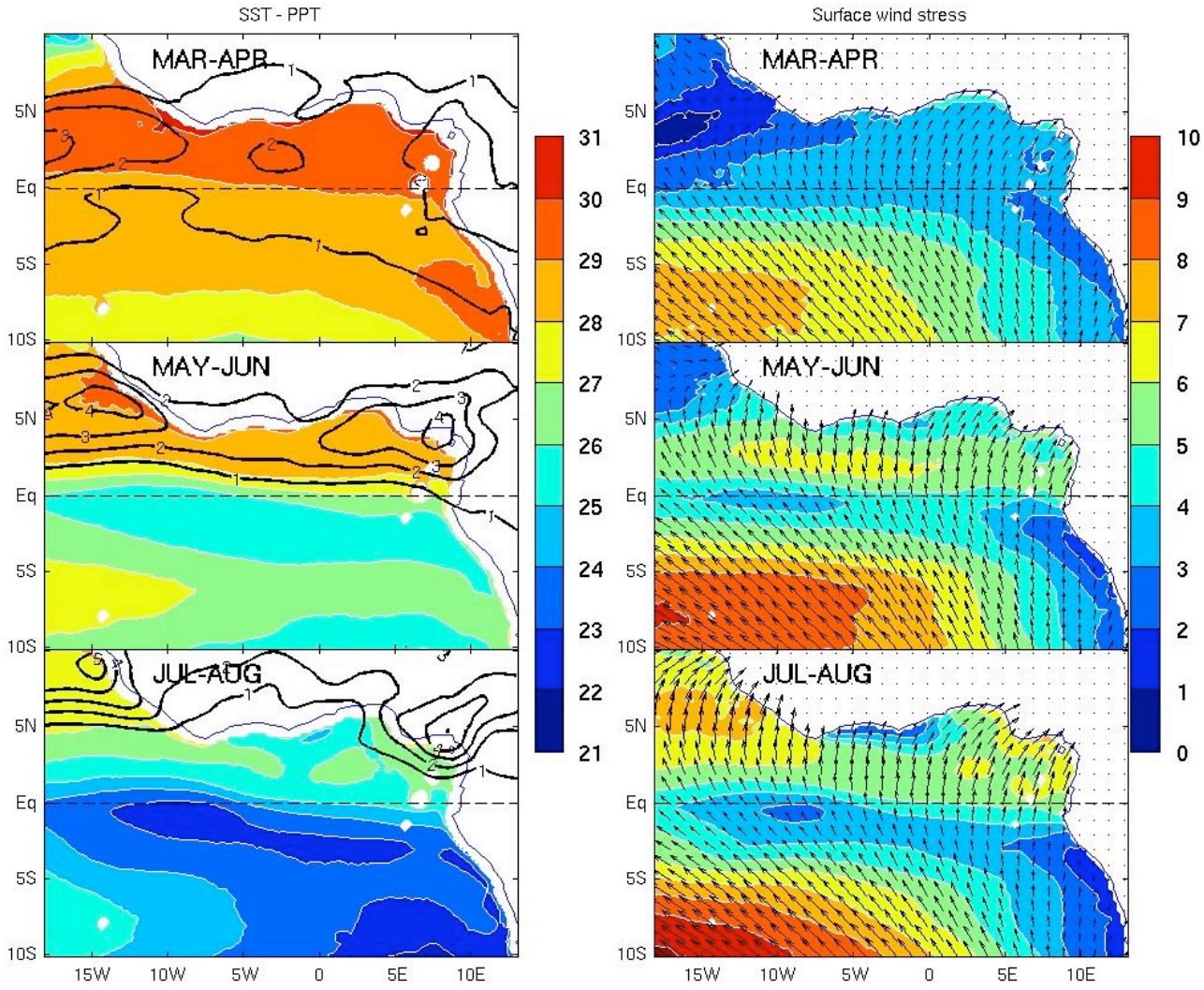

Figure 1. Left: 2000 - 2007 TMI SST (colours, °C) and TRMM rainfall (black contours, mm/day) monthly means. Right: 2000 – 2007 QuikSCAT surface wind-stress (one arrow on 16 plotted for clarity) with magnitude (colours, $\times 10^{-2} N/m^2$).

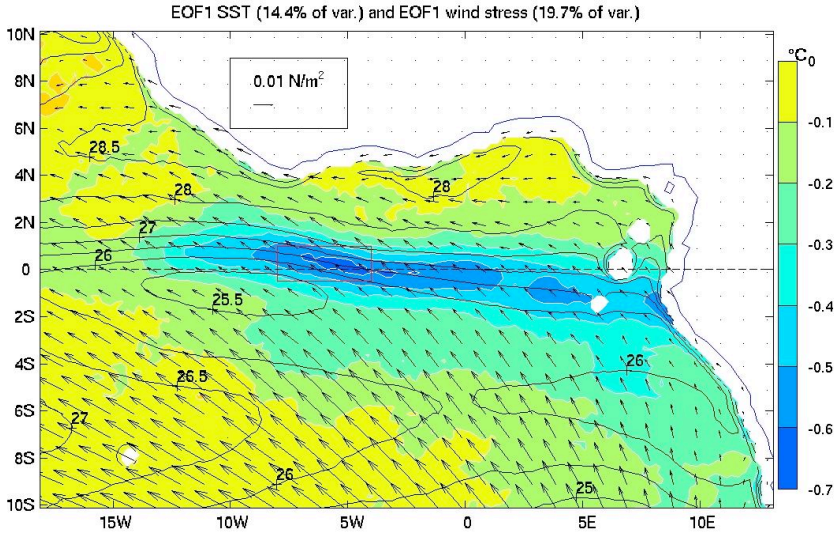

Figure 2: EOF 1 of SST TMI (°C, colours) and EOF 1 of QuikSCAT surface wind-stress (arrows). Black contours: mean SST TMI for MAMJJA 2000 – 2007 (°C).

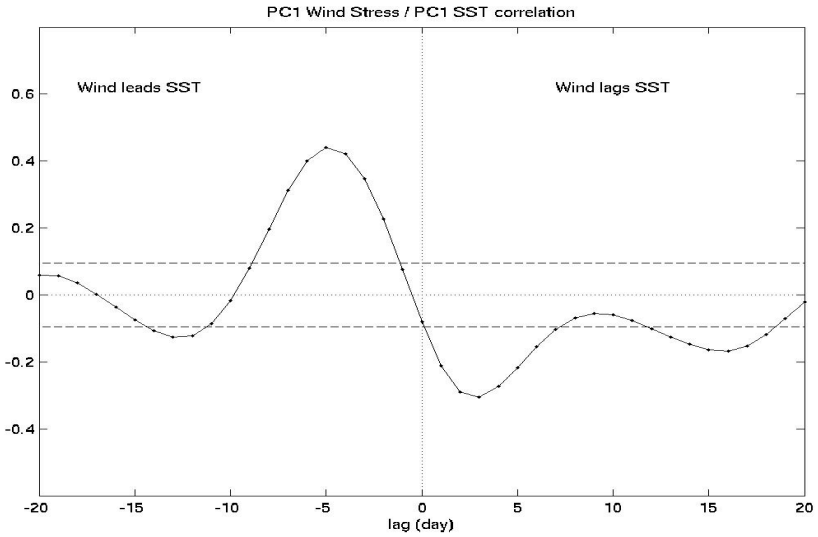

Figure 3: Lagged cross-correlation between first modes of SST and surface wind-stress (plain line) with 10% significant correlation (dashed lines). The atmosphere leads the ocean at negative lags.

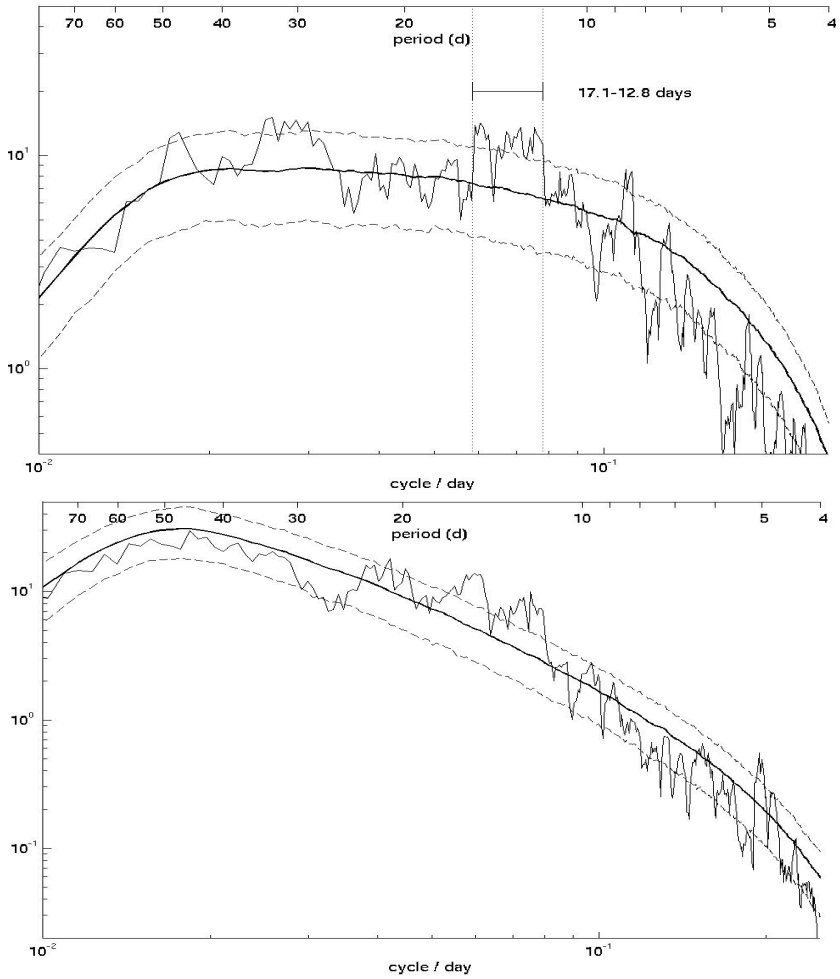

Figure 4: Top: 4-window multi-taper power spectrum of the first principal component of the surface wind-stress in the Gulf of Guinea. Heavy: mean spectrum of simulated AR1 of same variance and persistence. Dashed lines: 10 and 90% significance levels. Bottom: idem for the first principal component of the SST.

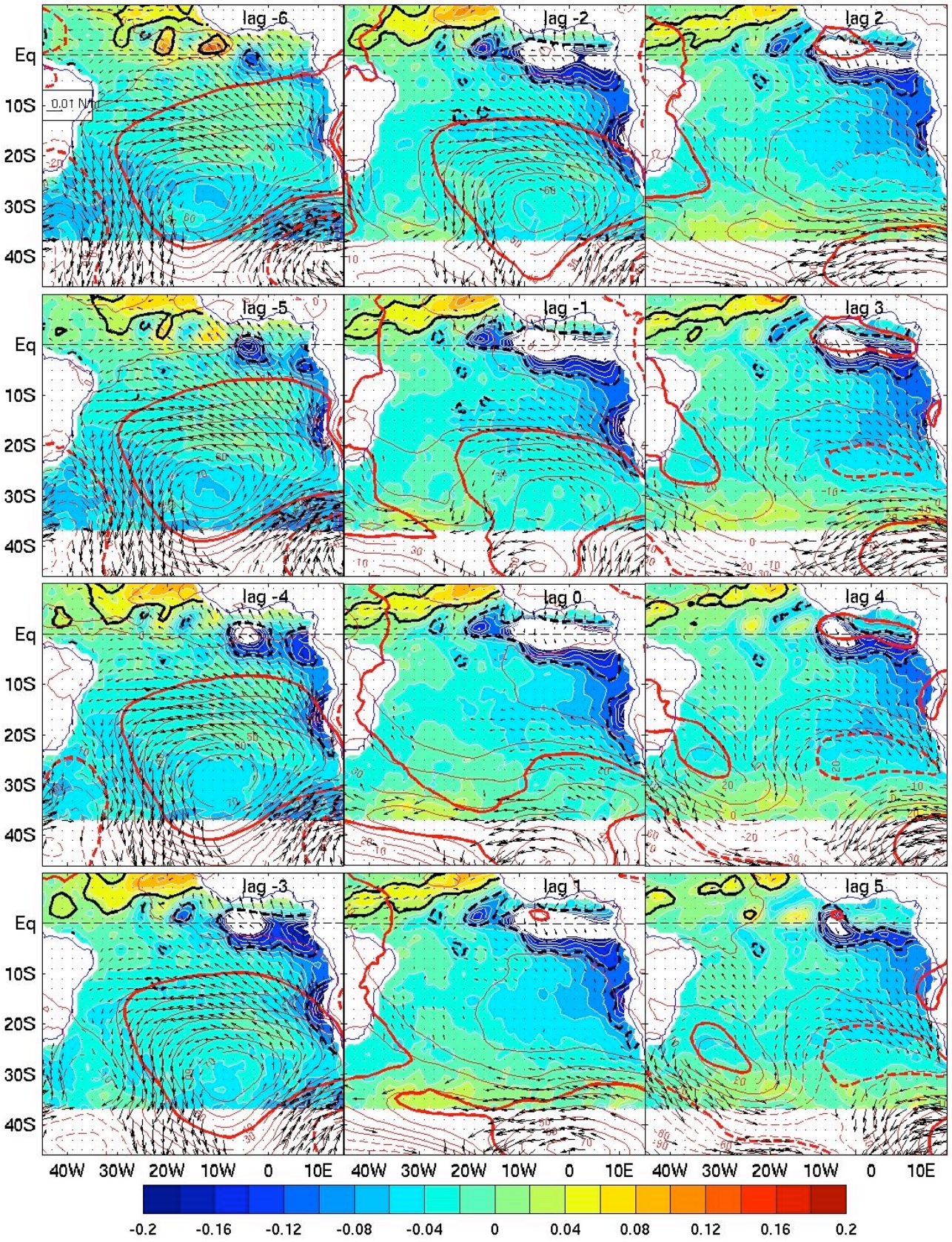

Figure 5: Lagged regression of QuikSCAT surface wind-stress (arrows, $N.m^{-2}$), ECMWF SLP (red contours, Pa) and TMI SST (colours, °C), on the CTI. Heavy black (resp. red) lines (plain for positive, dashed for negative) indicates the 10% level for point correlation between SST (resp. SLP) and the CTI. For clarity, SST colder than 0.2°C was left in blank and only one arrow on 4 plotted for the wind stress. The CTI lags (i.e. the atmosphere leads the ocean) at negative lags.

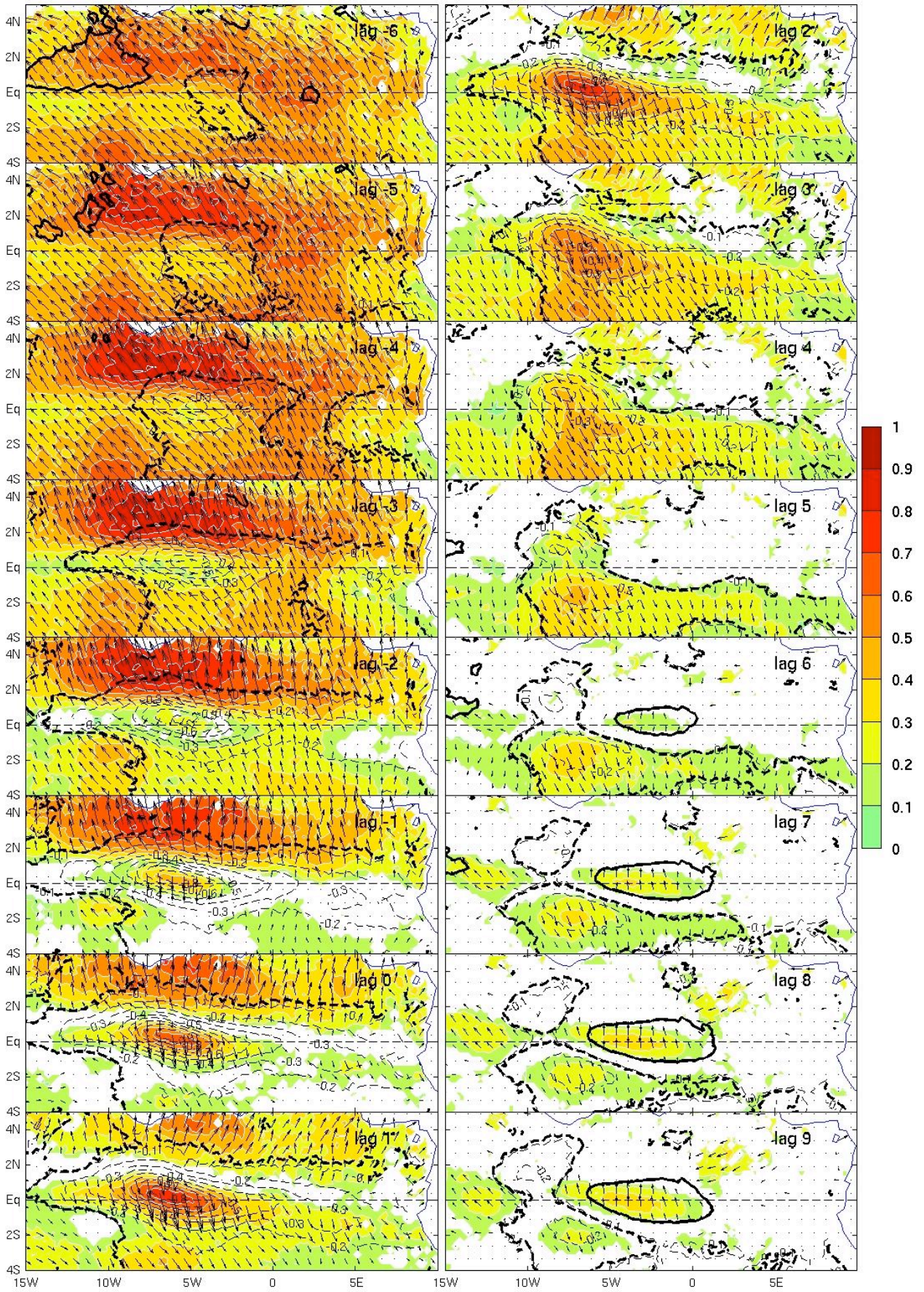

Figure 6: Lagged regression of QuikSCAT surface wind-stress (magnitude in colours, $\times 10^{-2} N.m^{-2}$), and ECMWF SST (black contours, intervals of 0.1°C) on the CTI. Only the winds above the 10% significant correlation level are plotted. Heavy contours (dashed for negative, plain for positive) indicate the 10% significant correlation for the SST projection. The CTI lags for negative lags.

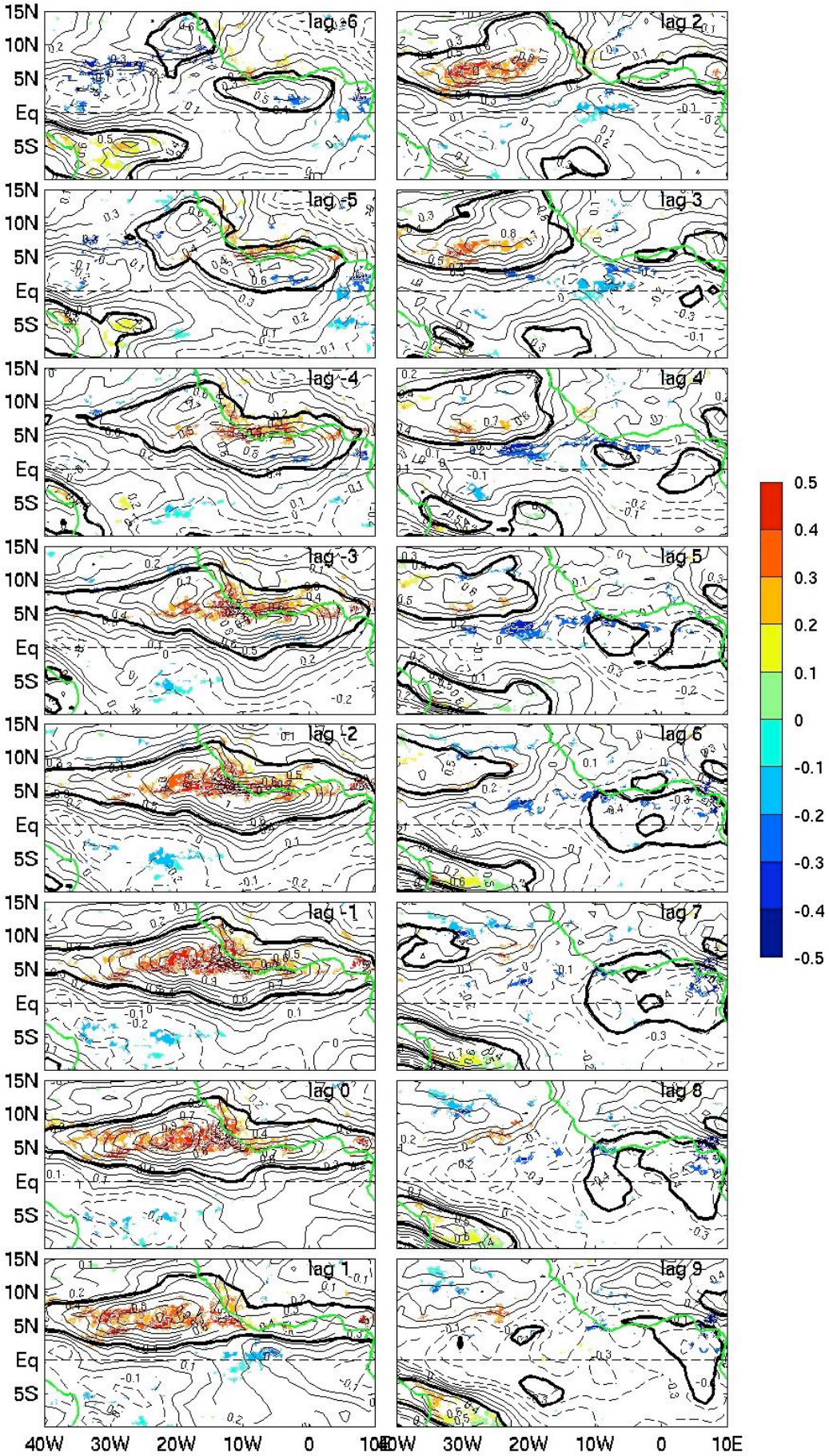

Figure 7: Lagged regression of TRMM rainfall (colours, mm/day) and Total Column Water Vapour (TCWV) in the ECWMF data (black contours, kg/m²) on the CTI. Heavy black contour indicates the 10% significant point correlation for TCWV. The CTI leads at negative lags. For clarity, coast lines are plotted in green.

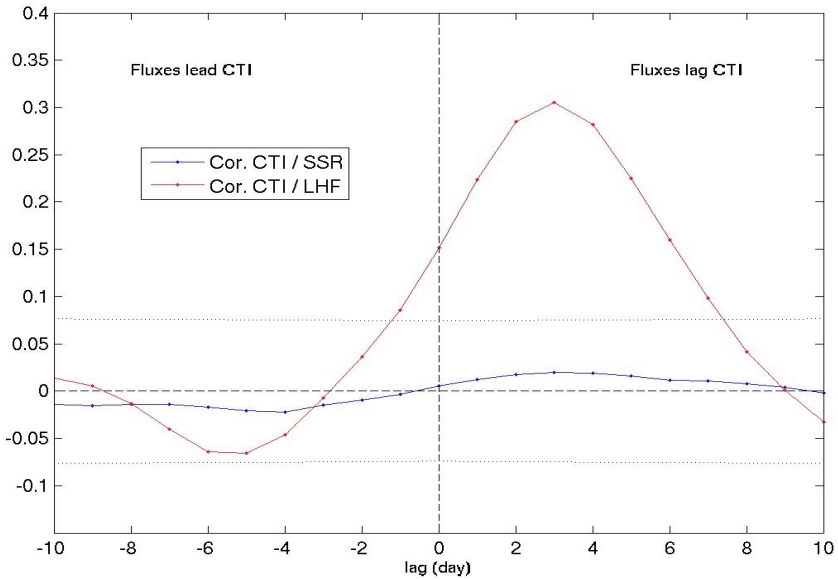

Figure 8: Lagged cross-correlation of the local ECMWF surface latent heat flux (red) and surface solar radiation (blue) with the CTI. The CTI leads at negative lags. 10% significant correlation plotted in dotted lines.

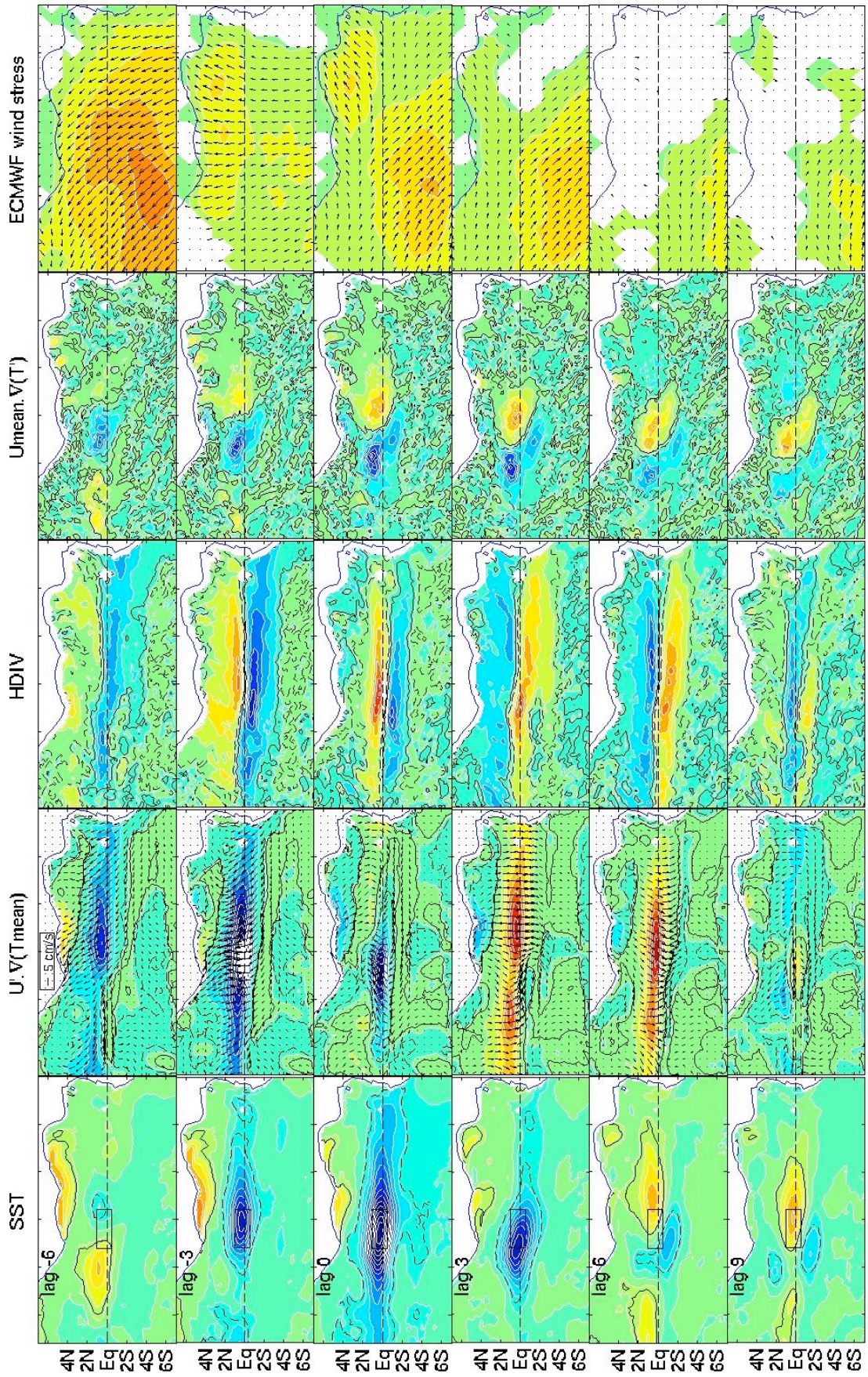

Figure 9: Lagged regression of SST (°C), $-U'.\nabla\overline{T}$ ($\times 10^{-7}\ °C.s^{-1}$) with surface currents ($m.s^{-1}$), HDIV ($\times 10^{-7}\ s^{-1}$, negative value means divergence), $-\overline{U}.\nabla T'$ ($\times 10^{-7}\ °C.s^{-1}$) and ECMWF surface wind-stress ($\times 10^{-2}\ N.m^{-2}$) to the CTI in the MERCATOR simulation. 10% significant correlation is plotted in plain (positive) or dashed (negative). Only the 10% significant currents and winds are plotted.

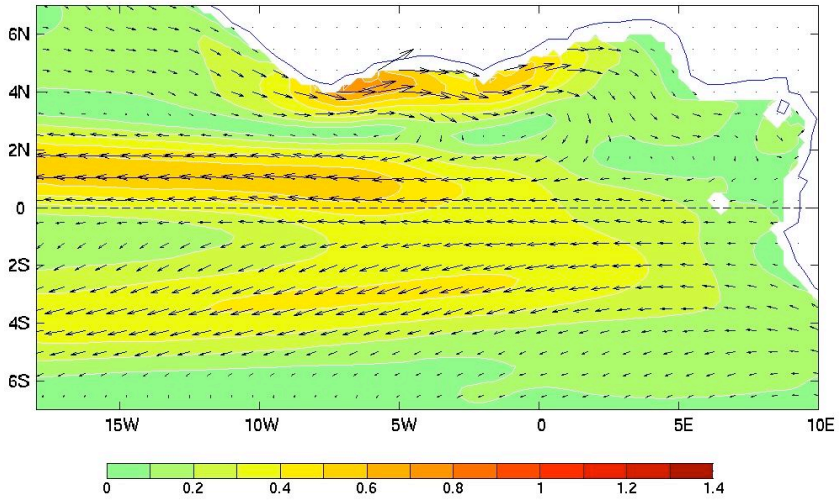

Figure 10: Mean surface currents in MAMJJA in the MERCATOR simulation ($m.s^{-1}$).